

# Safety Enhanced Boost Converter for PV Panel

Chintala Venkatesh<sup>1</sup>, G Vaddikasulu<sup>2</sup>

Assistant Professor, Department of Electrical Engineering, Atmakur Engineering College, Andhra Pradesh, India<sup>1</sup>

Assistant Professor, Department of Electrical Engineering, Atmakur Engineering College, Andhra Pradesh, India<sup>2</sup>

**ABSTRACT:** Within the photovoltaic (PV) power-generation market, the ac PV module has shown obvious growth. However, a high voltage gain converter is essential for the module's grid connection through a dc-ac inverter. This thesis proposes a converter that employs a floating active switch to isolate energy from the PV panel when the ac module is OFF; this particular design protects installers and users from electrical hazards. Without extreme duty ratios and the numerous turns-ratios of a coupled inductor, this converter achieves a high step-up voltage-conversion ratio; the leakage inductor energy of the coupled inductor is efficiently recycled to the load. These features explain the module's high-efficiency performance.

**KEYWORDS:** photovoltaic, coupled inductor, boost converter, safety.

## I. INTRODUCTION

PHOTOVOLTAIC (PV) power-generation systems are becoming increasingly important and prevalent in distribution generation systems. A conventional centralized PV array is a serial connection of numerous panels to obtain higher dc-link voltage for main electricity through a dc-ac inverter [1], [30]. Unfortunately, once there is a partial shadow on some panels, the system's energy yield become significantly reduced[2]. An ac module is a micro inverter configured on the rear bezel of a PV panel [1]–[3]; this alternative solution not only immunizes against the yield loss by shadow effect, but also provides flexible installation accordance with the user's budget[4]. Many prior research works have proposed a single-stage dc-ac inverter with fewer components to fit the dimensions of the bezel of the ac module, but their efficiency levels are lower than those of conventional PV inverters.

The power capacity a single PV panel is about 100W to 300W, and the maximum power point (MPP) voltage range is from 15V to 40V, which will be the input voltage of the ac module; in cases with lower input voltage, it is difficult for the ac module to reach high efficiency [3]. However, employing a high step-up dc-dc converter in the front of the inverter improves power conversion efficiency and provides a stable dc link to the inverter.

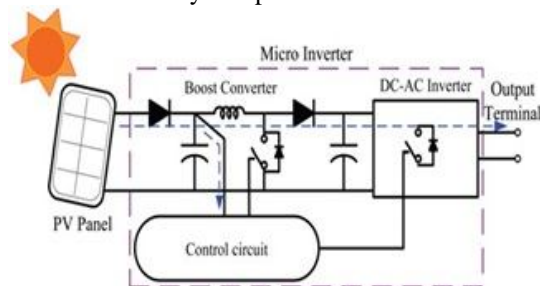


Fig.1. Potential difference on the output terminal of non floating switch micro inverter.

## International Journal of Innovative Research in Science, Engineering and Technology

(An ISO 3297: 2007 Certified Organization)

Vol. 4, Issue 8, August 2015

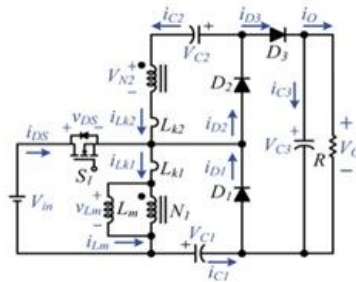


Fig. 2. Circuit configuration of proposed converter

Fig. 1 shows the solar energy through the PV panel and micro inverter to the output terminal when the switches are OFF. When installation of the ac module is taking place, this potential difference could pose hazards to both the worker and the facilities. A floating active switch is designed to isolate the dc current from the PV panel, for when the ac module is off-grid as well as in the non operating condition. This isolation ensures the operation of the internal components without any residential energy being transferred to the output or input terminals, which could be unsafe. The micro inverter includes dc–dc boost converter, dc–ac inverter with control circuit as shown in Fig. 1.

The dc–dc converter requires large step-up conversion from the panel's low voltage to the voltage level of the application. Previous research on various converters for high step-up applications has included analyses of the switched-inductor and switched-capacitor types [6],[7]; transformer less switched - capacitor type [8], [9]; the voltage-lift type; the capacitor-diode voltage multiplier; and the boost type integrated with a coupled inductor [10], these converters by increasing turns ratio of coupled inductor obtain higher voltage gain than conventional boost converter. Some converters successfully combined boost and fly back converters, since various converter combinations are developed to carry out high step-up voltage gain by using the coupled-inductor technique.

The efficiency and voltage gain of the dc–dc boost converter are constrained by either the parasitic effect of the power switches or the reverse-recovery issue of the diodes. In addition, the equivalent series resistance (ESR) of the capacitor and the parasitic resistances of the inductor also affect overall efficiency. Use of active clamp technique not only recycles the leakage inductor's energy but also constrains the voltage stress across the active switch, however the tradeoff higher cost and complex control circuit. By combining active snubber auxiliary resonant circuit, synchronous rectifiers, or switched- capacitor-based resonant circuits and soon, these techniques made active switch into zero voltage switching (ZVS) or zero current switching (ZCS) operation and improved converter efficiency. However, when the leakage- inductor energy from the coupled inductor can be recycled, the voltage stress on the active switch is reduced, which means the coupled inductor employed in combination with the voltage-multiplier or voltage-lift technique successfully accomplishes the goal of higher voltage gain [6]. The proposed converter, shown in Fig. 2, is comprised of a coupled inductor  $T_1$  with the floating active switch  $S_1$ . The primary winding  $N_1$  of a coupled inductor  $T_1$  is similar to the input inductor of the Conventional boost converter, and capacitor  $C_1$  and diode  $D_1$  receive leakage inductor energy from  $N_1$ . The secondary winding  $N_2$  of coupled inductor  $T_1$  is connected with another pair of capacitors  $C_2$  and diode  $D_2$ , which are in series with  $N_1$  in order to further enlarge the boost voltage. The rectifier diode  $D_3$  connects to its output capacitor  $C_3$ .

The proposed converter has several features:

- 1) The connection of the two pairs of inductors, capacitor, and diode gives a large step-up voltage-conversion ratio
- 2) The leakage-inductor energy of the coupled inductor can be recycled, thus increasing the efficiency and restraining the voltage stress across the active switch
- 3) The floating active switch efficiently isolates the PV panel energy during non operating conditions, which enhances safety. The operating principles and steady-state analysis of the proposed converter are presented in the following sections

# International Journal of Innovative Research in Science, Engineering and Technology

(An ISO 3297: 2007 Certified Organization)

Vol. 4, Issue 8, August 2015

## II. OPERATING PRINCIPLES OF THE PROPOSED CONVERTER

The simplified circuit model of the proposed converter is shown in Fig.2. The coupled inductor  $T_1$  is represented as a magnetizing inductor  $L_m$ , primary and secondary leakage inductors  $L_{k1}$  and  $L_{k2}$ , and an ideal transformer. In order to simplify the circuit analysis of the proposed converter, the following assumptions are made.

- 1) All components are ideal, except for the leakage inductance of coupled inductor  $T_1$ , which is being taken under consideration. The on-state resistance  $R_{DS(ON)}$  and all parasitic capacitances of the main switch  $S_1$  are neglected, as are the forward voltage drops of diodes  $D_1 \sim D_3$ .
- 2) The capacitors  $C_1 \sim C_3$  are sufficiently large that the voltages across them are considered to be constant.
- 3) The ESR of capacitors  $C_1 \sim C_3$  and the parasitic resistance of coupled inductor  $T_1$  are neglected.
- 4) The turn's ratio  $n$  of the coupled inductor  $T_1$  windings is equal to  $N_2/N_1$ .

The dc – dc converters are widely used in regulated switch mode dc supplies and in dc motor drive applications. The input to these converters is often an unregulated dc voltage, which is obtained by rectifying the line voltage and therefore it will fluctuate due to changes in the line voltage magnitude. Switch mode dc-dc converters are used to convert the unregulated dc input into a controlled dc output at a desired voltage level.

The operating principle of continuous conduction mode (CCM) is presented with the figures and current wave forms for continuous mode of operation as in figure 8. Here five modes of operation described with neat diagrams

### A.CCM Operation

**Mode I [ $t_0, t_1$ ]:** In this transition interval ,the magnetizing inductor  $L_m$  continuously charges capacitor  $C_2$  through  $T_1$  when  $S_1$  is turned ON. The current flow path is shown in Fig.3(a) switch  $S_1$  and diode  $D_2$  is conducting. The current  $i_{Lm}$  is decreasing because source voltage  $V_{in}$  crosses magnetizing inductor  $L_m$  and primary leakage inductor  $L_{k1}$ ; magnetizing inductor  $L_m$  is still transferring its energy through coupled inductor  $T_1$  to charge switched capacitor  $C_2$ , but the energy is decreasing; the charging current  $i_{D2}$  and  $i_{C2}$  are decreasing. The secondary leakage inductor current  $i_{Lk2}$  is declining as equal to  $i_{Lm} / n$ . Once the increasing  $i_{Lk1}$  equals decreasing  $i_{Lm}$  at  $t = t_1$ , this mode ends.

**Mode II [ $t_1, t_2$ ]:** During this interval, source energy  $V_{in}$  is series connected with  $N_2$ ,  $C_1$  and  $C_2$  to charge output capacitor  $C_3$  and load R; meanwhile magnetizing inductor  $L_m$  is also receiving energy from  $V_{in}$ . The current flow path is shown in Fig.3(b), where switch  $S_1$  remains ON and only diode  $D_3$  is conducting. The  $i_{Lm}$ ,  $i_{Lk1}$ , and  $i_{D3}$  are increasing because the  $V_{in}$  is crossing  $L_{k1}$ ,  $L_m$ , and primary winding  $N_1$ ;  $L_m$  and  $L_{k1}$  are storing energy from  $V_{in}$ ; meanwhile  $V_{in}$  is also serially connected with secondary winding  $N_2$  of coupled inductors  $T_1$ , capacitors  $C_1$ , and  $C_2$ , and then discharges their energy to capacitor  $C_3$  and load R. Then,  $i_{D3}$  and discharging current  $|i_{C1}|$  and  $|i_{C2}|$  are increasing. This mode ends when switch  $S_1$  is turned OFF at  $t = t_2$ .

**Mode III [ $t_2, t_3$ ]:** During this transition interval, secondary leakage inductor  $L_{k2}$  keeps charging  $C_3$  when switch  $S_1$  is OFF. The current flow path is shown in Fig.3(c) where only diode  $D_1$  and  $D_3$  are conducting. The energy stored in leakage inductor  $L_{k1}$  flows through diode  $D_1$  to charge capacitor  $C_1$  instantly when  $S_1$  is OFF. Meanwhile, the energy of secondary leakage inductor  $L_{k2}$  is series connected with  $C_2$  to charge output capacitor  $C_3$  and the load. Because leakage inductance  $L_{k1}$  and  $L_{k2}$  are far smaller than  $L_m$ ,  $i_{Lk2}$  rapidly decreases ,but  $i_{Lm}$  is increasing because magnetizing inductor  $L_m$  is receiving energy from  $L_{k1}$ . Current  $i_{Lk2}$  decreases until it reaches zero; this mode ends at  $t=t_3$ .

**Mode IV [ $t_3, t_4$ ]:** During this transition interval, the energy stored in magnetizing inductor  $L_m$  is released to  $C_1$  and  $C_2$  simultaneously. The current flow path is shown in Fig 3(d). Only diodes  $D_1$  and  $D_2$  are conducting. Currents  $i_0$  and  $i_{D1}$  are continually decreased because the leakage energy still flowing through diode  $D_1$  keeps charging capacitor  $C_1$ . The  $L_m$  is delivering its energy through  $T_1$  and  $D_2$  to charge capacitor  $C_2$ . The energy stored in capacitor  $C_3$  is constantly discharged to the load R. These energy transfers result in decreases in  $i_{Lk1}$  and  $i_{Lm}$  but increases in  $i_{Lk2}$ . This mode ends when current  $i_{Lk1}$  is zero at  $t=t_4$ .

**Mode V [ $t_4, t_5$ ]:** During this interval, only magnetizing inductor  $L_m$  is constantly releasing its energy to  $C_2$ . The current flow path is shown in Fig 3(e) which only diode  $D_2$  is conducting. The  $i_{Lm}$  is decreasing due to the magnetizing inductor energy flowing through the coupled inductor  $T_1$  to secondary winding  $N_2$ , and  $D_2$  continues to charge capacitor  $C_2$ . The energy stored in capacitor  $C_3$  is constantly discharged to the load R. This mode ends when switch  $S_1$  is turned ON at the beginning of the next switching period.

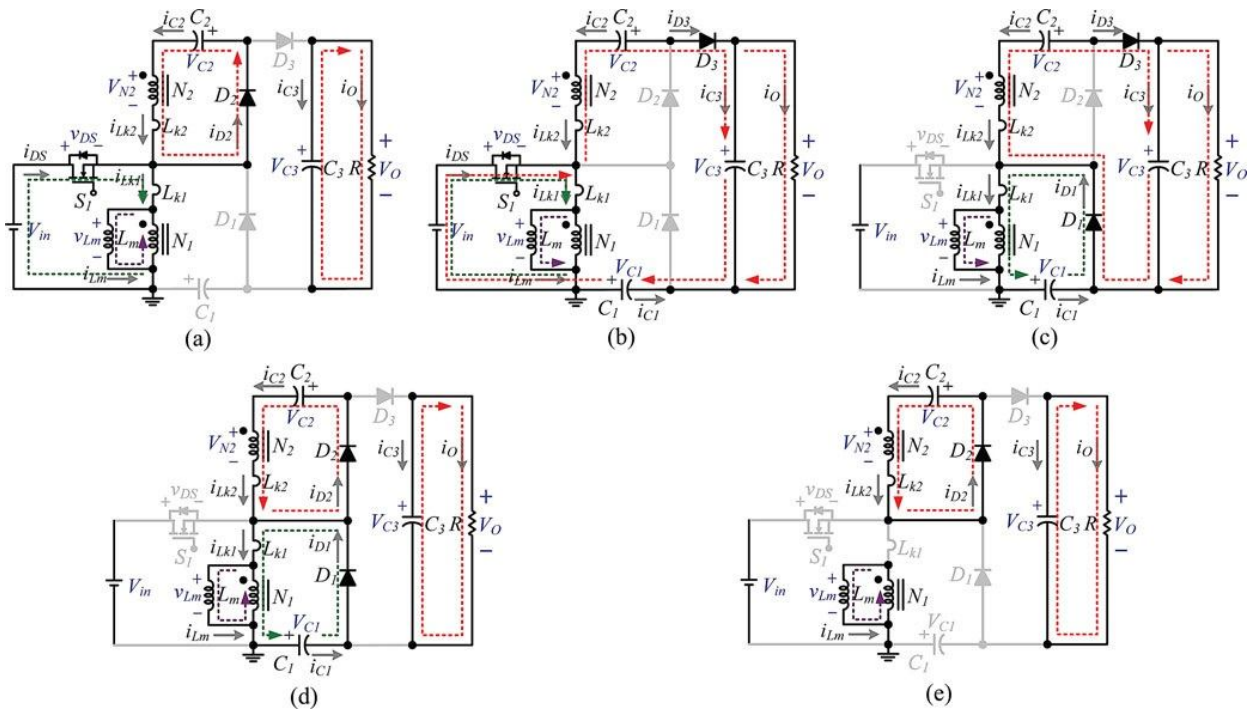


Fig. 3. Current flow path of five operating modes during one switching period at CCM operation. (a) Mode I:  $t_0 \sim t_1$ . (b) Mode II:  $t_1 \sim t_2$ . (c) Mode III:  $t_2 \sim t_3$ . (d) Mode IV:  $t_3 \sim t_4$ . (e) Mode V:  $t_4 \sim t_5$ .

### B. DCM Operation

The detailed operating principles for discontinuous- conduction-mode (DCM)operation represented in this section. Fig 5. Shows typical waveforms during five operating modes of one switching period. The operating modes are described as follows.

**Mode I [ $t_0, t_1$ ]:** During this interval, source energy  $V_{in}$  is series connected with  $N_2, C_1,$  and  $C_2$  to charge output capacitor  $C_3$  and load  $R$ ; meanwhile, magnetizing inductor  $L_m$  is also receiving energy from  $V_{in}$ . The current flow path is shown in Fig 6(a), which depicts that switch  $S_1$  remains ON, and only diode  $D_3$  is conducting. The  $i_{L_m}, i_{L_{k1}},$  and  $i_{D_3}$  are increasing because the  $V_{in}$  is crossing  $L_{k1}, L_m,$  and primary winding  $N_1$ ;  $L_m$  and  $L_{k1}$  are storing energy from  $V_{in}$ ; meanwhile,  $V_{in}$  also is serially connected with secondary winding  $N_2$  of coupled inductor  $T_1,$  capacitors  $C_1$  and  $C_2$  then they all discharge their energy to capacitor  $C_3$  and load  $R$ . The  $i_{in}, i_{D_3}$  and discharging current  $|i_{C1}|$  and  $|i_{C2}|$  are increasing. This mode ends when switch  $S_1$  is turned OFF at  $t = t_1$ .

**Mode II [ $t_1, t_2$ ]:** During this transition interval, secondary leakage inductor  $L_{k2}$  keeps charging  $C_3$  when switch  $S_1$  is OFF. The current flow path is shown in Fig 6(b), and only diode  $D_2$  and  $D_3$  are conducting. The energy stored in leakage inductor  $L_{k1}$  flows through diode  $D_1$  to charge capacitor  $C_1$  instantly when  $S_1$  is OFF. Meanwhile, the energy of secondary leakage inductor  $L_{k2}$  is series-connected with  $C_2$  to charge output capacitor  $C_3$  and the load. Because leakage inductance  $L_{k1}$  and  $L_{k2}$  are far smaller than  $L_m, i_{L_{k2}}$  decreases rapidly, but  $i_{L_m}$  is increasing because magnetizing inductor  $L_m$  is receiving energy from  $L_{k1}$ . Current  $i_{L_{k2}}$  reduces down to zero, and this mode ends at  $t = t_2$ .

**Mode III [ $t_2, t_3$ ]:** During this transition interval, the energy stored in coupled inductor  $T_1$  is releasing to  $C_1$  and  $C_2$ . The current flow path is shown in Fig 6(c). Only diodes  $D_1$  and  $D_2$  are conducting. Currents  $i_{L_{k1}}$  and  $i_{D_1}$  are continually decreased because leakage energy still flowing through diode  $D_1$  keeps charging capacitor  $C_1$ . The  $L_m$  is delivering its energy through  $T_1$  and  $D_2$  to charge capacitor  $C_2$ . The energy stored in capacitor  $C_3$  constantly discharged to the load  $R$ .

# International Journal of Innovative Research in Science, Engineering and Technology

(An ISO 3297: 2007 Certified Organization)

Vol. 4, Issue 8, August 2015

These energy transfers result in decreases in  $i_{Lk1}$  and  $i_{Lm}$  but increases in  $i_{Lk2}$ . This mode ends when current  $i_{Lk1}$  reaches zero at  $t = t_3$ .

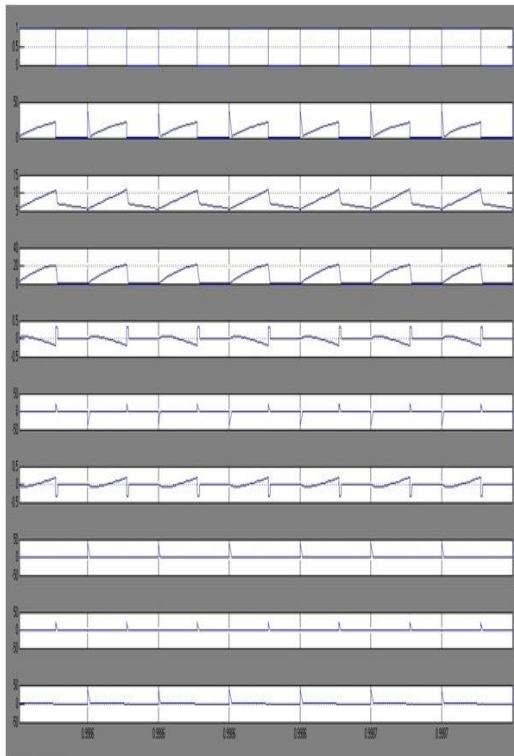


Fig. 4. Some typical waveforms of proposed converters at CCM operation

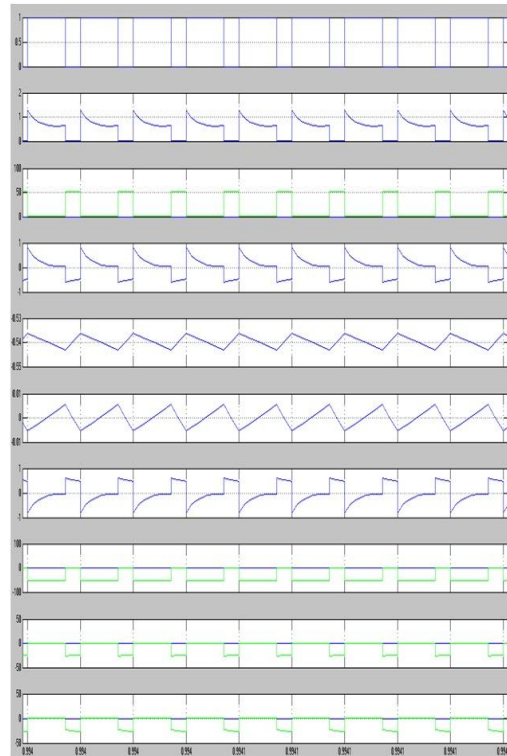


Fig. 5. Some typical waveforms of proposed converters at DCM operation

**Mode IV [ $t_3, t_4$ ]:** During this interval only magnetizing inductor  $L_m$  is constantly releasing its energy to  $C_2$ . The current flow path is shown in Fig 6(d) and only diode  $D_2$  is conducting. The  $i_{Lm}$  is decreasing due to the magnetizing inductor energy flowing through the coupled inductor  $T_1$  to secondary winding  $N_2$ , and  $D_2$  continues to charge capacitor  $C_2$ . The energy stored in capacitor  $C_3$  is constantly discharged to the load R. This mode ends when current  $i_{Lm}$  reaches zero at  $t=t_4$ .

**Mode V [ $t_4, t_5$ ]:** During this interval, all active components are turned OFF; only the energy stored in capacitor  $C_3$  is continued to be discharged to the load R. The current flow path is shown in Fig6(e). This mode ends when switch S1 is turned ON at the beginning of the next switching period.

### III. STEADY-STATE ANALYSIS OF PROPOSED CONVERTERS

#### A. Continuous-Conduction Mode (CCM)

In CCM, power transfer is a two-step process. When the switch is ON, stored energy builds in the inductor. When the switch is OFF, energy transfers to the output through the diode. The switch current is a stepped saw tooth with a fixed steady-state ON time with some amount of ripple current superimposed. During the ON time of the switch, if we assume zero losses for the moment, the voltage across the inductor is approximately the input voltage; and the voltage across the rectifier is the capacitor, or output voltage. When the switch turns OFF, the energy stored in the inductor releases into the output through the rectifier.



## International Journal of Innovative Research in Science, Engineering and Technology

(An ISO 3297: 2007 Certified Organization)

Vol. 4, Issue 8, August 2015

Equation above. This Equation holds true for CCM when the ripple current in the inductor is small relative to the average DC current. The equation is “close” when there is a high percentage of ripple current. Reassuringly, if the losses in Equation reduce to zero, the equation simplifies to the ideal case.

### B. Discontinuous-Conduction Mode (DCM)

In DCM, a switching cycle is composed of three intervals. The first two are the same as in CCM, where energy is stored in the inductor during the ON time of the switch, and transferred to the load during the OFF time of the switch. In DCM, however,

all of the energy in the inductor transfers to the load during this second interval. The third interval begins when the energy in the inductor is depleted, and terminates at the end of the switching period the next time the switch turns on. During this third interval the voltage across the inductor decays to zero, the voltage across the switch decays to the input voltage, and the in output voltage differential is across the rectifier. There is essentially no current flowing in the power stage during this interval.

Observe that since all of the energy in the inductor discharges in each switching cycle during an interval shorter than the  $(1 - D)$  conduction time, the peak current in the diode must be higher in DCM than in CCM. If the peak current is higher in the diode in DCM, then the peak current will be higher in the inductor and in the switch as well. With higher peaks and the same or a shorter conduction time, as a rule of thumb we can assume that for the same components, the RMS losses will be greater in a DCM converter than in an equivalent CCM converter.

The operating duty cycle of the converter in DCM dependent not only on the input and output voltages but on the inductor value and load current as well. In addition, in DCM operation, the current fall time (to zero) is usually different than  $(1 - D) \times T_s$ . To find the duty cycle in DCM, we can first find the fall time that is required to discharge the inductor by taking the peak current during the ON time and dividing it by the current’s rate of decay during the OFF time:

$$t_{fall} = \frac{m_{IL(ON)}}{-m_{IL(OFF)}} \times D \times T_s \quad (5)$$

The negative sign in the denominator of  $t_{fall}$  is due to the OFF-time slope being a negative value. If  $t_{fall}$  is less than  $(1 - D) \times T_s$ , the converter is operating in DCM. That is, if the time to discharge the energy in the inductor to zero is less than the OFF time of the switch, the converter is operating in DCM. Under this condition, the fall-time duty cycle,  $D_{disch}$ , is

$$D_{disch} = \frac{t_{fall}}{T_s} = \frac{V_{IN}}{V_{OUT} - V_{IN}} \times D_{DCM} \quad (6)$$

In steady-state operation, the average output current is equal to the average diode current. This average output current is equal to the peak current, averaged over the switching period

$$I_{OUT} = \frac{V_{IN}}{2L} \times T_s \times D_{DCM} \times D_{disch} \quad (7)$$

Solving for the DCM duty cycle results in

$$D_{DCM} = \frac{1}{V_{IN}} \sqrt{\frac{2L \times (V_{OUT} - V_{IN})}{T_s}} \times \sqrt{I_{OUT}} \quad (8)$$

If losses are included, the following is a slightly better approximation

# International Journal of Innovative Research in Science, Engineering and Technology

(An ISO 3297: 2007 Certified Organization)

Vol. 4, Issue 8, August 2015

$$D_{DCM} = \frac{1}{V_{IN} - \frac{((V_{OUT} + V_d) \times I_{OUT}) \times R_{tot}}{V_{IN}}} \times \sqrt{\frac{2L \times (V_{OUT} + V_d + V_{IN}) \times I_{OUT}}{T_s}} \quad (9)$$

## IV. EXPERIMENTAL RESULTS

A 100W prototype sample is presented to verify the practicability of the proposed converter. The electrical specifications are  $V_{in} = 15V$ ,  $V_O = 200V$ ,  $f_s = 50kHz$ , and full-load resistance  $R = 400 \Omega$ . The major components required are  $C1 = C2 = 47 \mu F$  and  $C3 = 220 \mu F$ . The main switch  $S_1$  is a MOSFET IXFK180N15P, the diodes  $D_1$  are MRB20200CTG, and the DPG30C300HB is selected for  $D_2$  and  $D_3$ . Since assign turns ratio  $n = 5$ , the duty ratio  $D$  is derived as 55%. The boundary normalized magnetizing inductor time constant  $\tau_{LB}$  is found by to be  $1.547 \times 10^{-3}$ . To define the proposed converter's BCM operation at 50% of the full load, the load resistance  $R = 800 \Omega$ . The boundary magnetizing inductance  $L_{mB}$  is found as follows:  $L_{mB} \cdot f_s R > 1.547 \times 10^{-3} \Rightarrow L_m > 24.75 \mu H$ .

The actual inductance of magnetizing inductor  $L_m$  of the coupled inductor is  $30.54 \mu H$ , which is larger than boundary magnetizing inductance  $24.75 \mu H$ . Fig.7 shows voltage and current waveforms, which are measured from active switch  $S_1$ , diodes  $D_1$ ,  $D_2$ , and  $D_3$ , and the current waveforms of  $C_1$  and  $C_2$ . The measured voltage spike across the active switch is found to be about 80V; this reveals that the energy of the leakage inductor has been stored in and voltage clamped by  $C_1$ .

These experimental waveforms agree with the operating principles and the steady-state analysis. Fig. 8 shows that the maximum efficiency of 95.3% occurred at 40% of full load; and the full-load efficiency is maintained at 92.3%. The efficiency variation is about 3%, and the flat efficiency curve is able to yield higher energy from the PV module during periods when sunlight is fading. The residential voltage discharge time of the proposed converter is 480 milliseconds, which prevents any potential electrical injuries to humans.

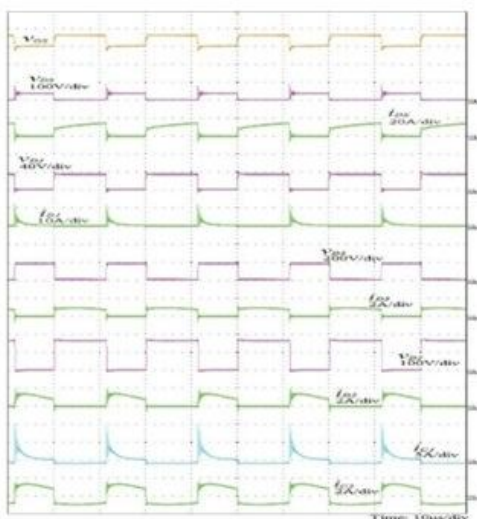


Fig7. Experimental waveforms measured by the condition of  $f_s = 50 \text{ kHz}$ ,  $V_{in} = 15 \text{ V}$ , and output 100.

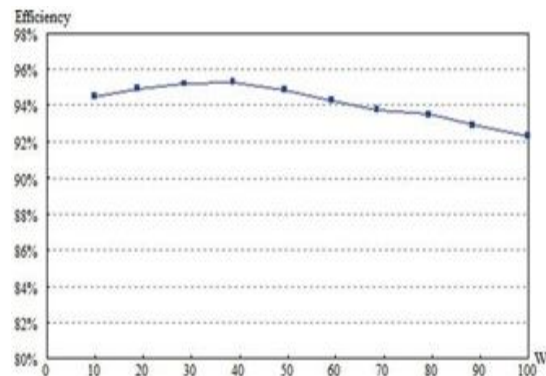


Fig. 8. Measured efficiency of proposed converter

# International Journal of Innovative Research in Science, Engineering and Technology

(An ISO 3297: 2007 Certified Organization)

Vol. 4, Issue 8, August 2015

## V. CONCLUSION

Since the energy of the coupled inductor's leakage inductor has been recycled, the voltage stress across the active switch  $S_1$  is constrained, which means low ON-state resistance  $R_{DS(O N)}$  can be selected. Thus, improvements to the efficiency of the proposed converter have been achieved. The switching signal action is performed well by the floating switch during system operation; on the other hand, the residential energy is effectively eliminated during the non operating condition, which improves safety to system technicians. From the prototype converter, the turns ratio  $n = 5$  and the duty ratio  $D$  is 53%; thus, without extreme duty ratios and turns ratios, the proposed converter achieves high step-up voltage gain, of up to 13 times the level of input voltage. The experimental results show that the maximum efficiency of 94% is measured at half load, and a small efficiency variation will harvest more energy from the PV module during fading sunlight.

## REFERENCES

- [1] T. Shimizu, K. Wada, and N. Nakamura, "Flyback-type single-phase utility interactive inverter with power pulsation decoupling on the dc input for an ac photovoltaic module system," *IEEE Trans. Power Electron.*, vol. 21, no. 5, pp. 1264–1272, Jan. 2006.
- [2] C. Rodriguez and G. A. J. Amaratunga, "Long-lifetime power inverter for photovoltaic ac modules," *IEEE Trans. Ind. Electron.*, vol. 55, no. 7, pp. 2593–2601, Jul. 2008.
- [3] S. B. Kjaer, J. K. Pedersen, and F. Blaabjerg, "A review of single-phase grid-connected inverters for photovoltaic modules," *IEEE Trans. Ind. Appl.*, vol. 41, no. 5, pp. 1292–1306, Sep./Oct. 2005.
- [4] J. J. Bzura, "The ac module: An overview and update on self-contained modular PV systems," in *Proc. IEEE Power Eng. Soc. Gen. Meeting*, Jul. 2010, pp. 1–3.
- [5] B. Jablonska, A. L. Kooijman-van Dijk, H. F. Kaan, M. van Leeuwen, G. T. M. de Boer, and H. H. C. de Moor, "PV-PRIVE project at ECN, five years of experience with small-scale ac module PV systems," in *Proc. 20<sup>th</sup> EurPhotovoltaic Solar Energy Conf.*, Barcelona, Spain, Jun. 2005, pp. 2728–2731.
- [6] T. Umeno, K. Takahashi, F. Ueno, T. Inoue, and I. Oota, "A new approach to low ripple-noise switching converters on the basis of switched-capacitor converters," in *Proc. IEEE Int. Symp. Circuits Syst.*, Jun. 1991, pp. 1077–1080.
- [7] B. Axelrod, Y. Berkovich, and A. Ioinovici, "Switched-capacitor/ switched-inductor structures for getting transformer less hybrid dc–dc PWM converters," *IEEE Trans. Circuits Syst. I, Reg. Papers*, vol. 55, no. 2, pp. 687–696, Mar. 2008.
- [8] B. Axelrod, Y. Berkovich, and A. Ioinovici, "Transformerless dc–dc converters with a very high dc line-to-load voltage ratio," in *Proc. IEEE Int. Symp. Circuits Syst. (ISCAS)*, 2003, vol. 3, pp. 435–438.
- [9] H. Chung and Y. K. Mok, "Development of a switched-capacitor dc–dc boost converter with continuous input current waveform," *IEEE Trans. Circuits Syst. I, Fundam. Theory Appl.*, vol. 46, no. 6, pp. 756–759, Jun. 1999.
- [10] T. J. Liang and K. C. Tseng, "Analysis of integrated boost-flyback

## BIOGRAPHY



**CH. Venkatesh** received his B.Tech. degree in Electrical and Electronics Engineering from JNTU University, Anantapur, Andhra Pradesh, India. He obtained M.Tech in Power Electronics from JNTU University, Anantapur, Andhra Pradesh, India. Presently he is working as an Assistant Professor in the Atmakur Engineering College, Nellore Palem, Nellore, Andhra Pradesh, India.



**G Vaddi kasulu** received his B.Tech. degree in Electrical and Electronics Engineering from JNTU University, Anantapur, Andhra Pradesh, India. He obtained M.Tech in Power Systems from JNTU University, Anantapur, Andhra Pradesh, India. Presently he is working as an Assistant Professor in the Atmakur Engineering College, Nellore Palem, Nellore, Andhra Pradesh, India.